**GUFBD / *GUJS* (2022) 12(3): 936-950**
DOI: 10.17714/gumusfenbil.1113019 Araştırma Makalesi / *Research Article*

# Investigation of ball milling effect on superconducting properties of oleic acid added bulk $MgB_2$ superconductors produced by two different methods

*İki farklı metot ile üretilen oleik asit katkılı külçe $MgB_2$ süperiletkenlerin süperiletkenlik özellikleri üzerine bilyeli öğütme etkisinin araştırılması*

**Özge ERDEM*[1, a]**
[1]*Bayburt University, Bayburt Vocational High School of Health Services, Department of Medical Services and Techniques, 69000, Bayburt*

• Geliş tarihi / *Received*: 06.05.2022 • Düzeltilerek geliş tarihi / *Received in revised form*: 25.06.2022 • Kabul tarihi / *Accepted*: 06.07.2022

**Abstract**
The effect of ball milling on the microstructure and some superconducting parameters such as flux pinning force (Fp) and critical current density (Jc) of the oleic acid ($C_{18}H_{34}O_2$) added $MgB_2$ bulk samples produced by two different methods, was analysed in this article. In the first method, ball milling was applied to the samples produced by using boron (B) powders coated with carbon (C) released from oleic acid. In the second method, oleic acid was mixed with magnesium (Mg) and B powders at the same time and then the same ball milling process used in the first method was applied to the powder mixture. The structural, magnetic and electrical properties of the produced samples were analysed. The results showed that ball milling process enhances the homogeneity of the structure, decreases the grain size and improves the grain connectivity of $MgB_2$. Also, C substitution into $MgB_2$ lattice resulting in an increase in electron scattering and disorders, enhances after ball milling process. It supplies a significant increase in Jc at high fields and causes a slightly decrease in transition temperature (Tc), especially for the samples produced by using the first method. Because the first method supports the ball milling effect on the homogenous dispersion of oleic acid addition in the $MgB_2$ structure and the C entrance to $MgB_2$ lattice, acting as pinning centres, the best Jc and Fp values at high fields was obtained for the produced samples with second method.

**Keywords:** Ball milling, Bulk superconductors, $MgB_2$, Oleic acid

***Öz***
*Bu makalede, iki farklı yöntem kullanılarak üretilen oleik asit ($C_{18}H_{34}O_2$) katkılı $MgB_2$ külçe örneklerin mikroyapı ile akı çivileme kuvveti (Fp) ve kritik akım yoğunluğu (Jc) gibi bazı süperiletkenlik parametreleri üzerine bilyalı öğütmenin etkisi incelenmiştir. Birinci yöntemde, oleik asitten salınan karbon (C) ile kaplanmış bor (B) tozları kullanılarak üretilen numunelere bilyalı öğütme uygulanmıştır. İkinci yöntemde oleik asit, magnezyum (Mg) ve B tozları ile aynı anda karıştırılmış ve daha sonra toz karışıma birinci yöntemde kullanılan aynı bilyalı öğütme işlemi uygulanmıştır. Üretilen numunelerin yapısal, manyetik ve elektriksel özellikleri analiz edilmiştir. Sonuçlar, bilyalı öğütme işleminin yapının homojenliğini arttırdığını, tane boyutunu küçülttüğünü ve $MgB_2$'nin tane bağlantısını iyileştirdiğini göstermiştir. Ayrıca, bilyalı öğütme sonrası elektron saçılması ve düzensizlikte artışa neden olan $MgB_2$ örgüsüne C yerleşimi artar. Bu durum, özellikle birinci yöntemle üretilen numunelerde yüksek alanlarda Jc'de önemli bir artış sağlar ve geçiş sıcaklığında (Tc) küçük bir azalmaya neden olur. Birinci yöntem, bilyalı öğütmenin oleik asit katkısının $MgB_2$ yapısına homojen dağılımı ve çivileme merkezleri görevi gören $MgB_2$ örgüsüne C girişi üzerindeki etkisini desteklediğinden, yüksek alanlarda en iyi Jc ve Fp değerleri ikinci yöntemle üretilen örnekler için elde edilmiştir.*

***Anahtar kelimeler**: Bilyalı öğütme, Külçe süperiletkenler, $MgB_2$, Oleik asit*

[*a] Özge ERDEM; ozgeerdem@bayburt.edu.tr, Tel: (0458) 211 11 71, orcid.org/0000-0003-4542-941X

## 1. Introduction
*1. Giriş*

The increasing energy need of the growing world population is one of the crucial problems of today. In order to meet the energy consumption and protect natural energy resources, it is necessary to develop systems that minimize energy loss and increase their practical applicability. Since the discovery of superconductivity, many devices (energy storage, magnetically levitated transportation vehicles (MAGLEV), magnetic bearing, etc.) have been produced to minimize energy losses caused by resistance and friction. One of the promising superconductors that can be used for this purpose is $MgB_2$.

$MgB_2$ is one of the low temperature superconductors with a remarkably high critical temperature ($T_c$). It is an intermetallic compound forming from magnesium (Mg) and boron (B). Considering that our country owns 73 % of the world's boron reserves, it is expected that $MgB_2$ superconductor-based researches will play a significant role in our country's energy development. In Turkey, boron powder with 99 % purity and boron based products are produced by Pavezyum company and sold to the world markets. Also, important organizations such as BOREN and BORTEK carry out crucial studies to expand the usage area of boron products.

From the discovery of superconductivity in $MgB_2$ till today, many studies have been reported on $MgB_2$ in bulk, thin film, tape and wire forms (Erdem & Yanmaz, 2015; Surdu et al., 2011; Sun et al., 2019). These studies are generally related on the topics of MRI systems (Majoros et al., 2022), superconducting generators (Wen et al., 2019), power cables (Klöppel et al., 2021), magnetic field shielding (Gozzelino et al., 2019), and magnetic levitation force (Erdem et al., 2020). The superconducting properties of $MgB_2$, such as high critical magnetic field ($H_{c2}$) and critical current density ($J_c$), must be enhanced for these applications to be successful. Due to the absence of inherent flux pinning centres, and the presence of high porosity and poor connectivity between the grains, the critical current density decreases so fast under a high field in $MgB_2$. The simplest and most effective ways to overcome this problem are adding or doping of chemicals to the $MgB_2$ structure and fabrication of $MgB_2$ with different methods such as hot pressing (Naito et al., 2020), ball milling (Liu et al., 2020), internal Mg diffusion technique (Kulich et al., 2016) and laser irradiation (Erdem & Yanmaz, 2017). Since the $MgB_2$ structure is resistant to many chemicals, the selection of the chemical powder to be used as an additive is very important. Carbon (C) released from C-containing compounds such as hydrocarbons can substitute into B site in the $MgB_2$ structure and as a result flux pinning performance improves (Erdem et al., 2017), without a substantial reduction in the critical temperature ($T_c$). Inside the production methods, ball milling is also a popular approach for improving $MgB_2$'s superconducting performance. Ball milling reduces the grain size of starting powders, improves grain connectivity (Liu et al., 2020) and bulk density, increases defects in the structure and ensures a uniform distribution of additives in $MgB_2$. As a result of functioning as pinning centres in the structure, the higher density of grain boundaries and defects in $MgB_2$ causes a rise in $J_c$.

In this study, oleic acid ($C_{18}H_{34}O_2$) was chosen as a chemical additive to increase the superconducting characteristics of bulk $MgB_2$ for practical applications. Oleic acid was wet mixed with B powder and B-Mg powder mixture to increase the homogeneity of $MgB_2$ structure, and then dried in the tube furnace. The obtained B powder coated with C and C-B-Mg powder mixture were ball milled for 2 h to look into the impact of ball milling on the oleic acid added $MgB_2$ produced with two different methods. The reason of the selection of oleic acid among the fatty acids as an additive is because of that it is an active C resource for $MgB_2$ and it can bind effectively to the un-oxidized boron surface with homogenous distribution providing a complete protection against air oxidation for B (Van Devener et al., 2009). Oleic acid is a C-rich organic source releasing C from a long hydrocarbon chain at temperatures below those required for $MgB_2$ production. It is a colourless to pale yellow liquid with a mild odour. It is produced naturally by the body. It has a low melting point like about 13°C-16°C. It is insoluble in water and soluble in methanol and ethanol. In the literature, there are two articles reported on the oleic acid added $MgB_2$ wire (Martinez et al., 2013; Laliena et al., 2015). In these articles, $MgB_2$ in wire form was investigated and the effects of ball milling and oleic acid addion on the critical current density of $MgB_2$ wires were examined. Unlike these studies, the ball milling effect was researched on the oleic acid added bulk $MgB_2$ samples produced by two different ways in this article. The phase composition, microstructure, magnetic and electrical properties of oleic acid added and milled samples were examined in detailed, then the results were compared with the pure and un-milled samples. It is thought that the results obtained from

this study can be a guide for other researchers working on the contribution of organic acids to the $MgB_2$ superconductor.

## 2. Material and method
*2. Materyal ve metot*

In this study, the bulk $MgB_2$ samples with oleic acid addition at the rate of 0 %, 5 % and 10 % by weight of 1 g $MgB_2$ were produced with two different methods by following the steps given below.

In the first method, B powder and oleic acid in liquid form (56 µlt and 112 µlt) were wet mixed in an appropriate stoichiometric ratio and ground in an agate mortar in air for 30 minutes. The mixture was dried in an aluminium oxide (alumina) crucible under 0.5 bar argon (Ar) atmosphere at 400°C for 1 h using a tube furnace. Thus, it was ensured that the B powder was coated with C, and the excess oleic acid in the structure was removed by evaporating, not the oleic acid that was directly bound to the B particles. The obtained B powder coated with C released from the oleic acid was then mixed with Mg powder according to the desired stoichiometric ratio. In addition, 5 wt % extra Mg powder was incorporated into the powder mixture to take advantage of the vapour pressure of Mg and to prevent stoichiometry shifts as a result of Mg evaporation during the sintering process. 1 gr powder mixture was pressed using an automatic pressing machine under 10 tons at 200°C. The pressing temperature was adjusted with a programmable temperature controller. The mould was kept at 200°C for 30 minutes under pressure. The $MgB_2$ samples were obtained as a pellet form with 5 mm in thickness and 13 mm in diameter by cooling the hot mould to room temperature under pressure. The $MgB_2$ pellets were placed one by one in a small chrome tube for sintering. The end of chrome tube was closed by welding and inside the furnace, the tube was inserted in a huge chrome tube. The oxygen in the tube was removed by vacuuming and a 1 bar Ar atmosphere was created in the tube. In a tube furnace, the pellets were sintered for 2 hours at 850°C. As a result, the three bulk $MgB_2$ samples named as A-0, A-5 and A-10 were produced with B particles coated with C using 0 %, 5 % and 10 % oleic acid ratios by weight of 1 gr $MgB_2$, respectively. To examine the influence of ball milling on superconducting characteristics of $MgB_2$ produced with first method, $ZrO_2$ milling balls with a 1:20 powder mass-ball mass ratio was added to the B coated with C-Mg powder mixture obtained in the first method before pressing process. The powder mixture was ball milled in a $ZrO_2$ bowl using a ball milling machine with a rotation speed of 200 rpm for 2 h. To prevent the powder mixture from the oxidation that may occur due to heating during ball milling, the machine was stopped for 1 min. every 3 min. and the rotation direction was changed automatically. After ball milling, pressing and sintering processes used in the first method were applied to the powder mixture. Thus, two bulk $MgB_2$ samples produced by using ball milling were obtained with 5 wt % and 10 wt % oleic acid additions and named respectively as AM-5 and AM-10.

In the second method, Mg, B and oleic acid were mixed in a proper stoichiometric ratio and were ground for 30 minutes in an agate mortar in air. Then in an aluminium oxide (alumina) crucible, the wet powder mixture was dried under 0.5 bar Ar atmosphere at 400°C for 1 h. In order to determine ball milling effect, the dried mixture was milled for 2 h with a 1:20 powder mass-ball mass ratio and a rotation speed of 200 rpm, as in the first method. After ball milling, pressing and sintering processes used in the first method were applied to the powder mixture. With this second method, only 10 wt % oleic acid added bulk $MgB_2$ sample with 1 gr named as BM-10 was produced.

One can see all the oleic acid added bulk $MgB_2$ samples produced in this study from Table 1.

**Table 1.** Oleic acid added bulk $MgB_2$ samples produced in this study
***Tablo 1.*** *Bu çalışmada üretilen oleik asit katkılı külçe $MgB_2$ örnekler*

| Samples | Oleic acid content (wt %) | Ball milling (h) |
|---|---|---|
| A-0 | 0 | - |
| A-5 | 5 | - |
| A-10 | 10 | - |
| AM-5 | 5 | 2 |
| AM-10 | 10 | 2 |
| BM-10 | 10 | 2 |

### 2.1. Analysis
*2.1. Analizler*

X-ray diffractometer (λ=1,5418 Å) with $CuK_\alpha$ radiation was used for phase determination and peak analysis of the produced samples. The measurements were taken with a scanning speed of 0.2°/min in the range of 2Θ = 10°-80°. From the XRD measurements, the lattice parameters *a* and *c* were determined. The peak shifting was analysed

also for all the samples. Scanning electron microscopy (SEM) analysis was also carried out to determine ball milling effect on the grain size, grain connectivity and grain boundaries of $MgB_2$.

The studied samples were cut into a rectangular shape and magnetization versus magnetic field intensity, $M(H)$ measurements were taken at 5 K and 20 K under ± 7 T with 50 Oe/s sweep speed by using physical properties measurement system (PPMS). The critical current density values of the samples depending on the magnetic field, $J_c(\mu_0 H)$ were calculated using the magnetization loops obtained from $M(H)$ measurements and Bean's critical state model (Bean, 1962) given by the equation $J_c = 20\Delta M / [a\,(1 - (a / 3b))]$. Here, $\Delta M$ is in emu/cm$^3$, $a$ and $b$ are in cm ($a < b$) and $J_c$ is in A/cm$^2$. The flux pinning force values as a function of magnetic field, $F_p(B)$ were obtained by using $F_p = J_c \times B$ equation. Here, $F_p$ is in N/m$^3$. The $T_c$ values for the produced samples were determined from the magnetic moment depending on temperature curves, $m(T)$. The $m(T)$ measurements were performed from 300 K to 5 K at $H$ = 100 Oe by using PPMS.

Resistivity versus temperature, $\rho(T)$ measurements of the samples were taken when the applied magnetic field was at $B$ = 0 T. The variation observed in resistivity was recorded while the samples were cooling from 300 K to 10 K. The values of intrinsic residual resistivity ($\rho_0$) and residual resistivity ratio ($RRR$) were calculated using the resistivity values at 40 K and 300 K ($\rho_{40\,K}$, $\rho_{300\,K}$) and $B$ = 0 T. The $\rho_0$ values were calculated from the equation $\rho_0 = K \times \rho_{40\,K}$ (Matsushita et al., 2008). Here, $K$ is the electrical connectivity and given as $K = \Delta\rho_g / \Delta\rho$. The value of $\Delta\rho_g$ is 4.3 μΩcm for a good pure single crystal (Eltsev et al., 2002), and $\Delta\rho$ is equal to $\Delta\rho = \rho_{300\,K} - \rho_{40\,K}$. The equation of $RRR = \rho_{300\,K} / \rho_{40\,K}$ was also used to determine the $RRR$ values (Jiang et al., 2006).

## 3. Results and discussion
*3. Bulgular ve tartışma*

Figure 1a-f show the XRD patterns of A-0, A-5, A-10, AM-5, AM-10, and BM-10 samples, respectively. The $MgB_2$ peaks shown in Figure 1a represent the (001), (100), (101), (002), (110), (102), (111), (200), (201) phases, respectively. The main phase for all the samples is $MgB_2$ and small MgO peaks is also observed. The MgO peaks shown in Figure 1a represent the (111), (220) and (222) phases, respectively. A-5 and A-10 samples show a relatively high intensity of MgO peak than the samples ball milled. Thus, it can be said that main phase is preserved for the oleic acid added samples and there is not a specific effect of oleic acid on the phase formation of $MgB_2$. Also, contrary to expectations, ball milling does not increase the oxidation in the $MgB_2$ structure.

Figure 2a and b respectively illustrate the lattice parameters $a$ and $c$ versus the oleic acid content for the A-0, A-5, A-10, AM-5, AM-10, and BM-10 samples. In literature, the $a$ and $c$-axis parameters are respectively given as 3.086 Å and 3.524 Å (Buzea & Yamashita, 2001). The values of $a$ and $c$ parameters obtained for the A-0 reference sample are a bit higher than that of the literature because of the production method. When the Figure 2a and b are analysed, it is seen that the $a$-lattice parameter decreases when the amount of oleic acid is increased for the oleic acid added samples compared with the A-0 reference sample. The increase-decrease trend in the $c$-lattice parameter is not systematic for the studied samples. The decrement of $a$-lattice parameter indicates that the C released from the oleic acid substitutes into the B sites in the $MgB_2$ lattice (Takenobu et al., 2001). Due to the different atomic sizes of C and B atoms, C substitution acting as pinning centres, causes disorders and strain in the lattice. The reason for the sharp reduce in the $a$-axis for the A-10 sample is the reduction of crystallinity due to the presence of large amount of C in the structure.

The variation of (110) peak depending on the amount of oleic acid for the bulk $MgB_2$ samples produced in this study is shown in Figure 3. The (110) peak observed at approximately 59.9°, represents in-plane scattering and is used to determine the $a$-lattice parameter. It is seen from Figure 3 that the peak intensity of (110) decreases and the peak position shifts to big angles as the oleic acid amount increases. These changes observed in (110) peaks are an indication of a decrease in $a$-lattice parameter (Kazakov et al. 2005) and the increase in the density of intra-plane disorders because the C substituted to $MgB_2$ lattice introduces the lattice disorders in the ab plane (Das et al., 2015). The intensity of (110) peak decreases more for the A-5 and A-10 un-milled samples comparing to the AM-5, AM-10 and BM-10 milled samples, because of more degradation of crystallinity for the un-milled samples with the oleic acid addition.

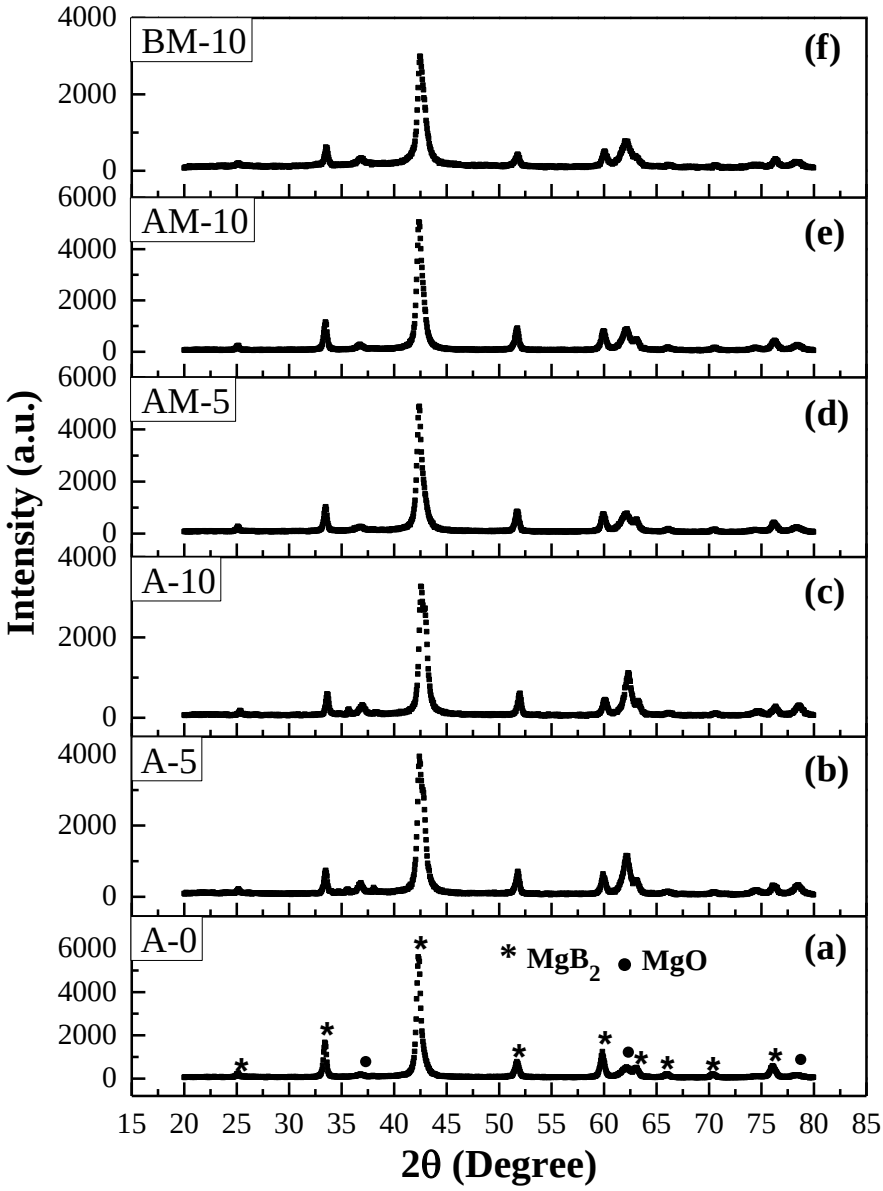


**Figure 1.** (a-f) XRD patterns of the A-0, A-5, A-10, AM-5, AM-10, and BM-10 oleic acid added bulk $MgB_2$ samples, respectively.
***Şekil 1.*** *(a-f) Sırasıyla A-0, A-5, A-10, AM-5, AM-10 ve BM-10 oleic asit katkılı külçe $MgB_2$ örneklerin XRD desenleri*

Figure 4a-f show the SEM images of the A-0, A-5, A-10, AM-5, AM-10, and BM-10 samples, respectively. Compared to the A-0 reference sample, it is seen that the structure shows an agglomeration for the A-5 and A-10 un-milled samples because of the oleic acid does not disperse homogenously in the structure (see Figure 4b and c), while the microstructure gains a denser appearance with small-sized grains, homogeneity increases and grain connectivity improves for the AM-5, AM-10 and BM-10 ball milled samples (see Figure 4d-f). It is known that the strong grain connectivity provides strong pinning performance at high fields which is essential for high $J_c$ values (Wu et al., 2006). In addition, the density of grain boundaries increases because of the reduction of grain size due to the ball milling. The $J_c$ value for the ball milled samples is projected to rise since the major pinning mechanism in $MgB_2$ is grain boundaries.

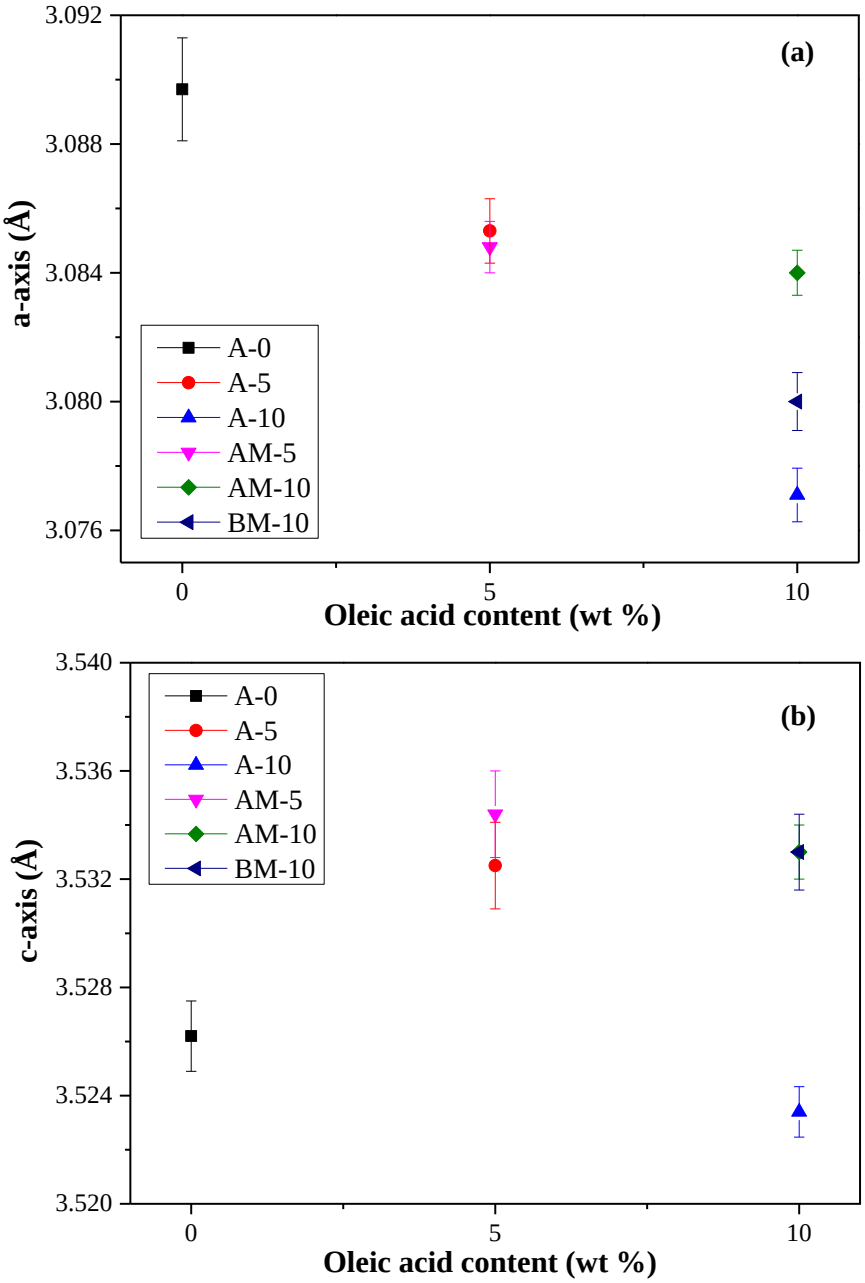


**Figure 2.** Variation of (a) *a* and (b) *c* lattice parameters versus oleic acid content for the A-0, A-5, A-10, AM-5, AM-10, and BM-10 samples.
***Şekil 2.*** *A-0, A-5, A-10, AM-5, AM-10 ve BM-10 örnekleri için oleik asit miktarına karşı (a) a ve (b) c örgü parametrelerinin değişimi.*

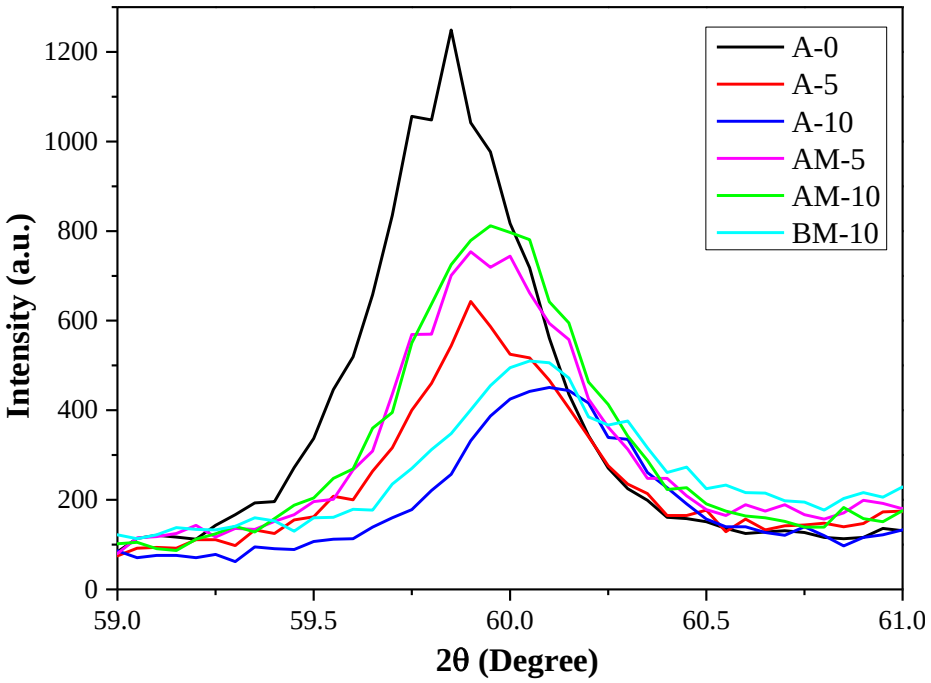


**Figure 3.** Variation of peak position and intensity of (110) peak observed at 59.9° for the A-0, A-5, A-10, AM-5, AM-10, and BM-10 samples.
***Şekil 3.*** *A-0, A-5, A-10, AM-5, AM-10 ve BM-10 örnekleri için 59.9°'de gözlenen (110) pikinin pik pozisyonunda ve şiddetindeki değişim*

The $J_c$ curves at 5 K and 20 K figured out from $M(H)$ loops, shown as inside figures, are given in Figure 5a and b, respectively. From the inside figure, it is seen that there is a flux jump in the magnetization curves at 5 K. As the magnetic diffusion rate becomes faster than the thermal diffusion rate at low temperature, magnetic flux abruptly moves to cause flux jumps (Kimishima et al., 2007). The hysteresis loops observed in Figure 5a and b are due to flux trapping in the samples and have a supporting role on $J_c$ parameter. When the $J_c$ curves at 5 K are examined in detail, it is seen that all the oleic acid added samples show a small $J_c$ value at low magnetic fields until 3.5 T, compared to the A-0 reference sample. When $\mu_0 H$ > 3.5 T, the AM-5 and AM-10 ball-milled samples show the highest $J_c$ values. In addition, for $\mu_0 H$ > 5 T the $J_c$ values are higher for all the samples than that of the A-0 reference sample. A similar behaviour is seen in the $J_c$ curves at 20 K in Figure 5b. For $\mu_0 H$ > 2.5 T at 20 K, the AM-10 sample shows the highest $J_c$ value. For $\mu_0 H$ > 4.5 T the $J_c$ values are higher for all the oleic acid added samples than that of the A-0 reference one. One can see from Table 2 the $J_c$ values at 6 T, 5 K and 4 T, 20 K for all the produced samples. The highest $J_c$ values are respectively observed at 5 K for the AM-10, AM-5, BM-10, A-5, A-10 and A-0 samples. The highest $J_c$ values for AM-10 sample are 2.60 × $10^4$ A/cm$^2$ at 6 T, 5 K and 1.04 × $10^4$ A/cm$^2$ at 4 T, 20 K. These $J_c$ values are respectively about 3 times and 2.6 times higher than that of the A-0 reference sample, and about 2.8 times and 2.5 times higher than that of the A10 un-milled sample. In addition, the $J_c$ value at 6 T, 5 K of AM-10 bulk sample which was ball milled for 2 h with a 1:20 powder mass-ball mass ratio and a rotation speed of 200 rpm, is compatible with the $J_c$ value of W10B-MB wire sample with 10 wt % oleic acid addition and ball milled for 3 h with a 1:26 powder mass-ball mass ratio and a rotation speed of 400 rpm, as reported by Laliena et al. (2015).

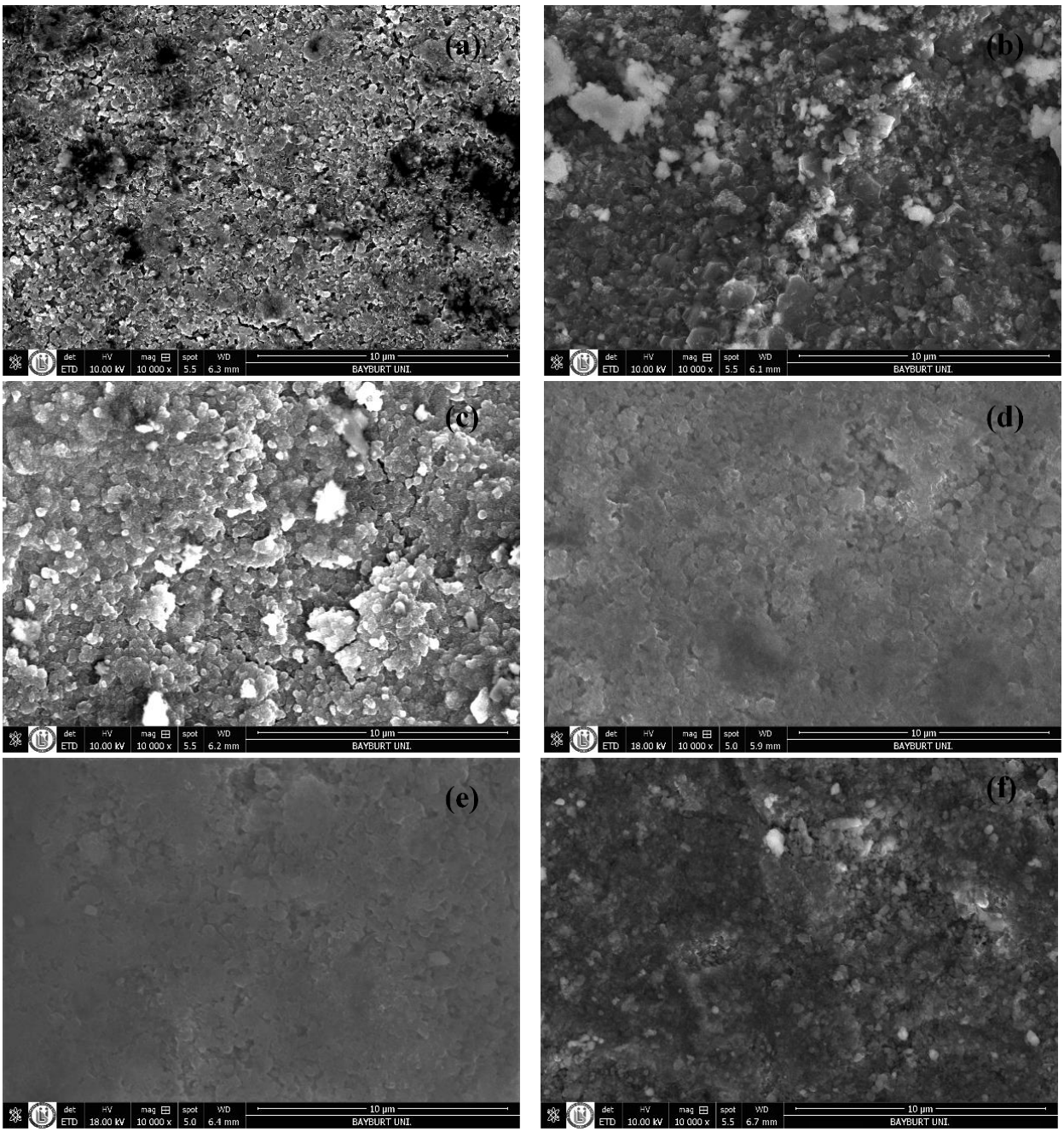


**Figure 4.** (a-f) SEM images of the A-0, A-5, A-10, AM-5, AM-10, and BM-10 samples, respectively.
***Şekil 4.*** *(a-f) Sırasıyla A-0, A-5, A-10, AM-5, AM-10 ve BM-10 örneklerinin SEM görüntüleri*

In this study, the $J_c$ values of all the AM-5, AM-10, BM-10 ball milled samples at 5 K for $\mu_0 H > 5$ T are higher compared with the $J_c$ values of A-0, A-5 and A-10 un-milled samples. This result differs from that reported by Laliena et al. (2015). The $J_c$ value at 5 K for W10B-MB ball-milled wire sample is lower until approximately for $\mu_0 H > 8.5$ T than that of the un-milled sample. Thus, it can be concluded that the selected ball milling parameters used in this study is significantly effective in the increment of $J_c$ values at high fields. In addition, comparing the $J_c$ values of AM-5, AM-10 and BM-10 samples given in Table 2, one can say that ball milling is more effective for the first method used in this study to enhance the $J_c$ value at high fields for both measurement temperatures.

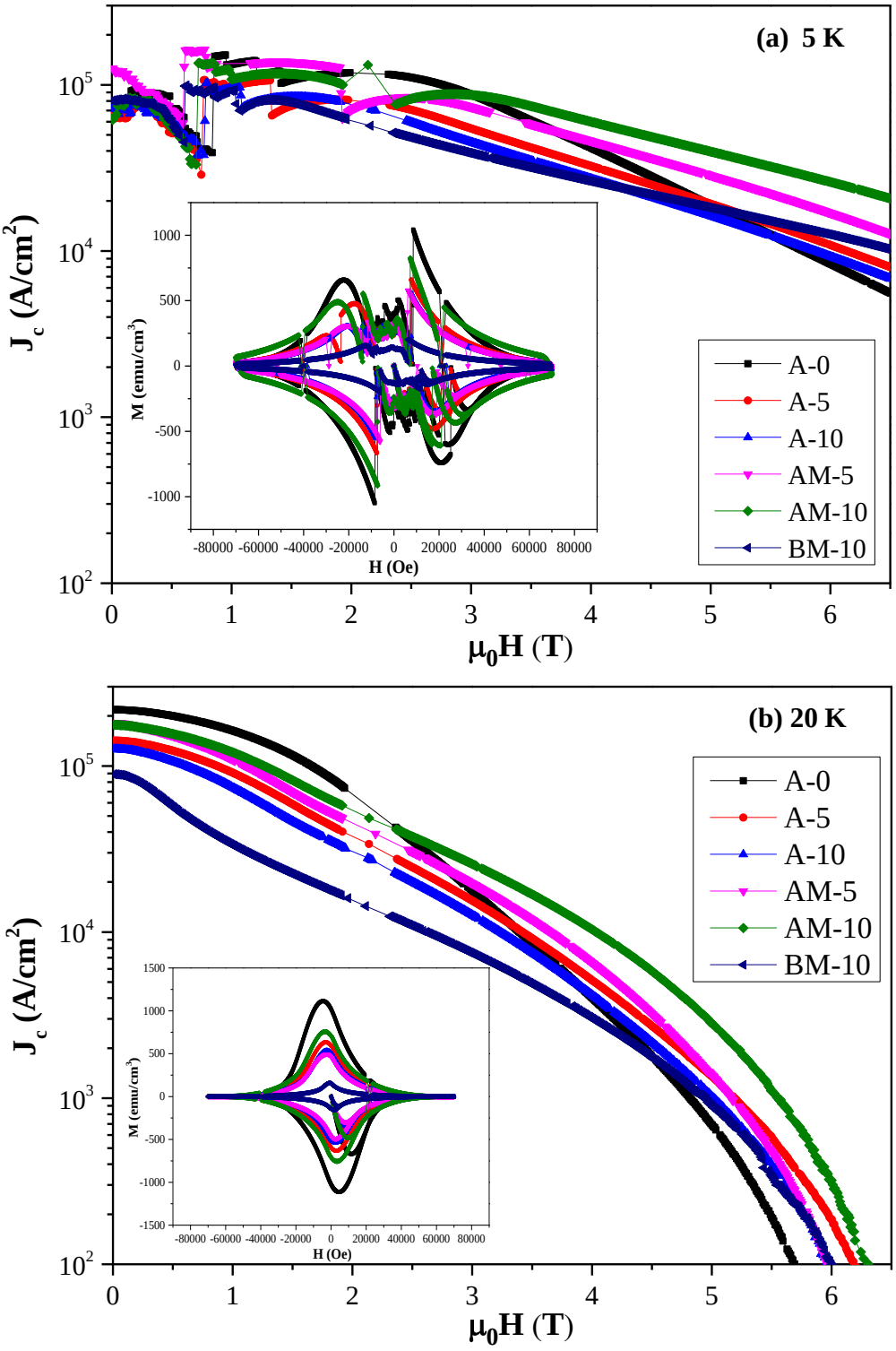


**Figure 5.** The $J_c$ curves calculated from the $M(H)$ loops shown in the inside figures for the A-0, A-5, A-10, AM-5, AM-10, and BM-10 samples at (a) 5 K and (b) 20 K.
***Şekil 5.*** *A-0, A-5, A-10, AM-5, AM-10 ve BM-10 örnekleri için (a) 5 K ve (b) 20 K'de iç şekillerde gösterilen M(H) çevriminden hesaplanan $J_c$ eğrileri*

To investigate the flux pinning performance of the produced samples in detailed, the $F_p$ values were calculated from the $J_c$ curves shown in Figure 5 and the $F_p(\mu_0 H)$ curves were plotted in Figure 6a and b at 5 K and 20 K, respectively. The A-0 reference sample shows the highest $F_p$ values for the low field regions at 5 K and 20 K, among the other samples. For $\mu_0 H > 5$ T and $\mu_0 H > 4.5$ T, similar to the results obtained from Figure 5, the $F_p$ values are respectively higher at 5 K and 20 K for the samples with oleic acid addition than that of the A-0 reference sample. As a result of these findings, the

increment of $J_c$ values is attributed to the strong flux pinning performance of the oleic acid added samples at high fields, and also homogenous structure and strong grain connectivity, especially observed in the ball-milled samples (see Figure 4d-f). The highest $F_p$ value is obtained for the AM-10 sample at both measurement temperatures and high fields, compatible with the results obtained from Figure 4 and Figure 5.

**Table 2.** The $J_c$ values at 6 T, 5 K and at 4 T, 20 K for the A-0, A-5, A-10, AM-5, AM-10, and BM-10 samples, respectively.
***Tablo 2.*** *Sırasıyla A-0, A-5, A-10, AM-5, AM-10 ve BM-10 örnekleri için 6 T, 5 K ve 4 T, 20 K'deki $J_c$ değerleri.*

| **Samples** | **$J_c$ (6 T, 5K) (A/cm$^2$)** | **$J_c$ (4 T, 20 K) (A/cm$^2$)** |
|---|---|---|
| A-0 | $0.83 \times 10^4$ | $0.40 \times 10^4$ |
| A-5 | $1.08 \times 10^4$ | $0.52 \times 10^4$ |
| A-10 | $0.92 \times 10^4$ | $0.42 \times 10^4$ |
| AM-5 | $1.69 \times 10^4$ | $0.65 \times 10^4$ |
| AM-10 | $2.60 \times 10^4$ | $1.04 \times 10^4$ |
| BM-10 | $1.25 \times 10^4$ | $0.30 \times 10^4$ |

Figure 7a illustrates the magnetic moment depending on temperature, $m(T)$ curves between 30 K and 300 K for the A-0, A-5, A-10, AM-5, AM-10, and BM-10 samples. In order to define the $T_c$ values from the $m(T)$ curves, the curves are plotted between 35 K and 40 K, as shown in Figure 7b. For the A-0, A-5, A-10, AM-5, AM-10, and BM-10 samples, the $T_c$ values are respectively obtained as 38.14 K, 37.87 K, 38.27 K, 38.63 K, 37.88 K and 37.64 K. For the A-10 oleic acid added and un-milled sample, the $T_c$ value is almost same as that of the A-0 reference sample. It implies that the C content substituted to the $MgB_2$ lattice is much less than in other samples. Compared with the A-0 reference sample, the $T_c$ value increases about 0.5 K for the AM-5 ball milled sample, because of the enhancing homogeneity and grain connectivity, as shown in Figure 4d. For the AM-10 and BM-10 samples, the $T_c$ values decrease because of more C content substituted into the lattice. The decrease observed in $T_c$ value is more prominent in the BM-10 sample produced with second method.

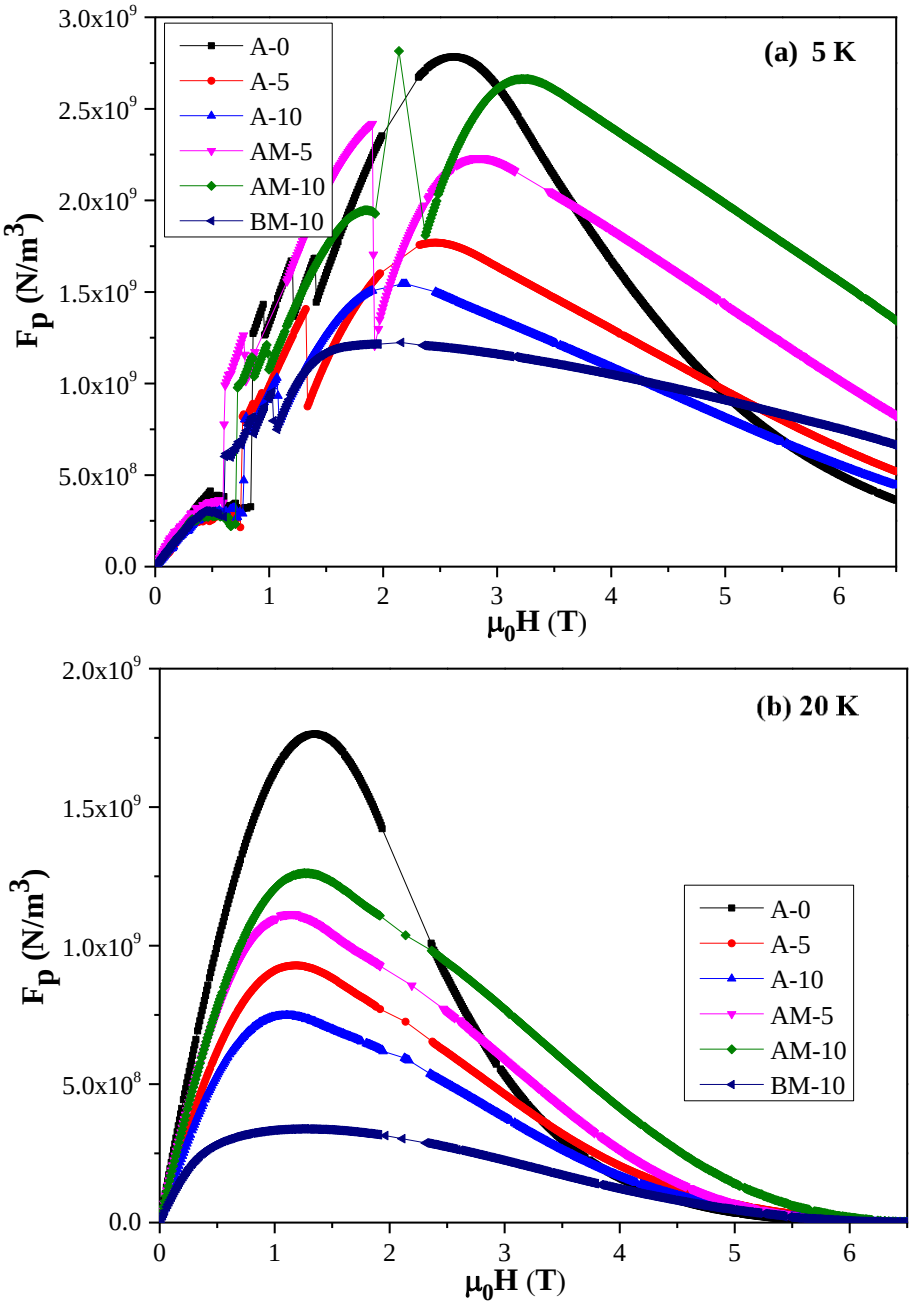


**Figure 6.** The flux pinning force density curves versus the magnetic field, $F_p(\mu_0 H)$ for the A-0, A-5, A-10, AM-5, AM-10, and BM-10 samples at (a) 5 K and (b) 20 K

***Şekil 6.*** *A-0, A-5, A-10, AM-5, AM-10 ve BM-10 örnekleri için (a) 5 K ve (b) 20 K'de manyetik alana karşı akı çivileme kuvvet yoğunluğu eğrileri,* $F_p(\mu_0 H)$.

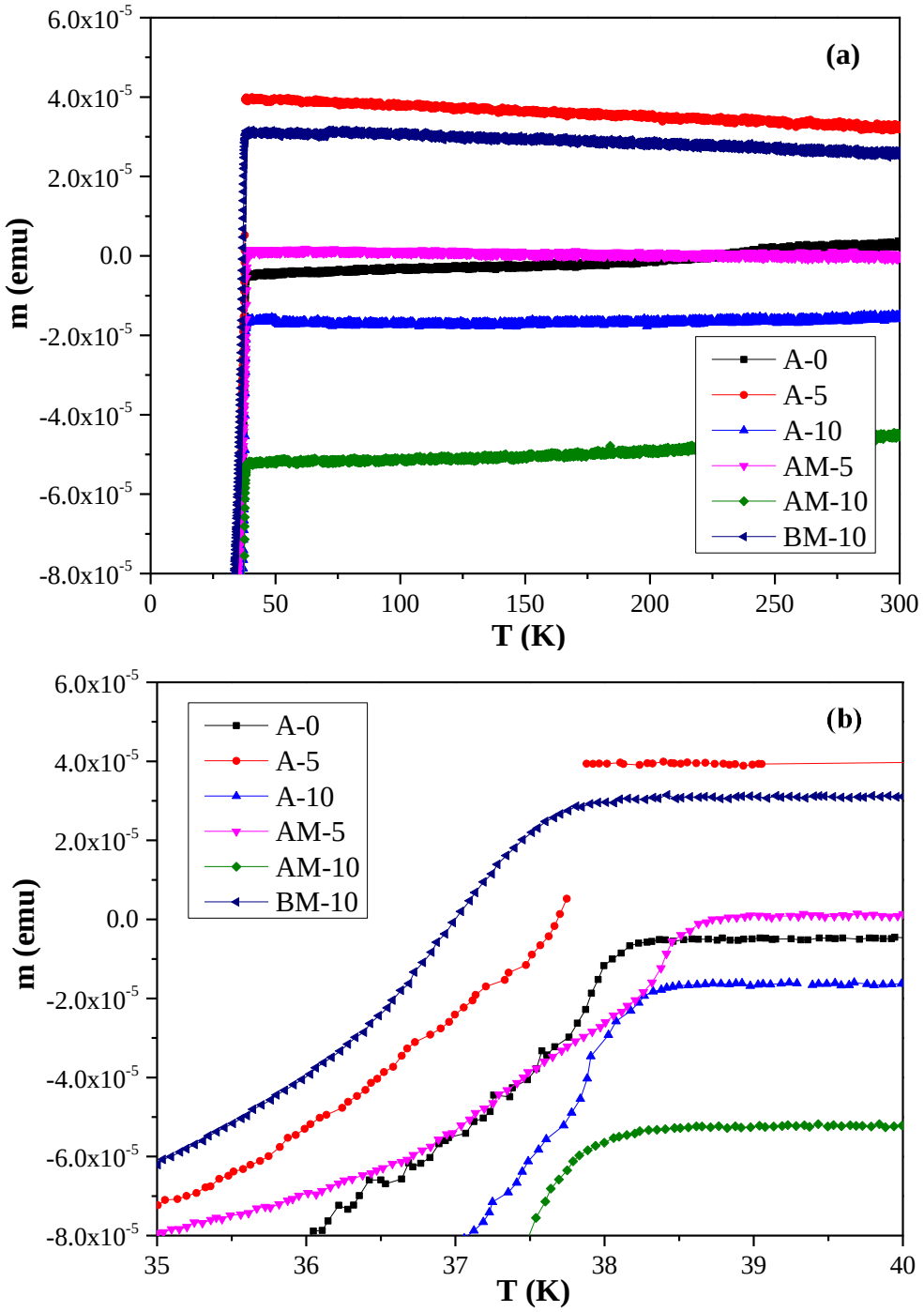


**Figure 7.** Magnetic moment depending on temperature, $m(T)$ curves between (a) 30 K and 300 K and (b) 35 K and 40 K for the A-0, A-5, A-10, AM-5, AM-10, and BM-10 samples.
***Şekil 7.*** *A-0, A-5, A-10, AM-5, AM-10 ve BM-10 örnekleri için (a) 30 K ve 300 K ve (b)35 K ve 40 K aralığında sıcaklığa bağlı manyetik moment, m(T) eğrileri.*

The temperature dependence of resistivity, $\rho(T)$ curves between 300 K and 10 K for the A-0, A-5 and AM-5 samples are illustrated in Figure 8. The resistivity curves are intermittent for the temperature values at which the transition to zero resistivity is observed for the samples. Therefore, the $T_c$ values of the samples could not be determined from the $\rho(T)$ curves. The values of residual resistivity ratio (*RRR*) and intrinsic residual resistivity ($\rho_0$) for the A-0, A-5 and AM-5 samples were calculated by using the resistivity values at $B$ = 0 T obtained from Figure 8. The values of $\rho_{40K}$, $\rho_{300K}$, $\Delta\rho$, $\rho_0$ and *RRR* are given in Table 3. Because the ball milling process enhances the C substitution and the density of defects in the structure, the resistivity values of $\rho_{40\,K}$ and $\rho_{300\,K}$ of the AM-5 ball milled sample are the highest among the other samples. In addition, the $\rho_0$ value is the highest for the AM-5 sample, indicating that the mean free path of carries has become about 1.3

times shorter than that of the A-0 reference sample due to the enhanced electron scattering because of more C substitution into the lattice resulting in an increase in $H_{c2}$ and thus $J_c$ (Ye et al., 2014). The increment of $\rho_0$ value is compatible with the decrement of *RRR* value for the AM-5 sample. The decrease observed in *RRR* value indicates that the electron scattering and the lattice disorders increase owing to more C substitution to B sites (Das et al., 2015). The RRR value is higher for the A-5 sample because the residual C that does not entrance the lattice, enhances the *RRR* value. These results imply that the ball milling improves the C substitution into the $MgB_2$ lattice.

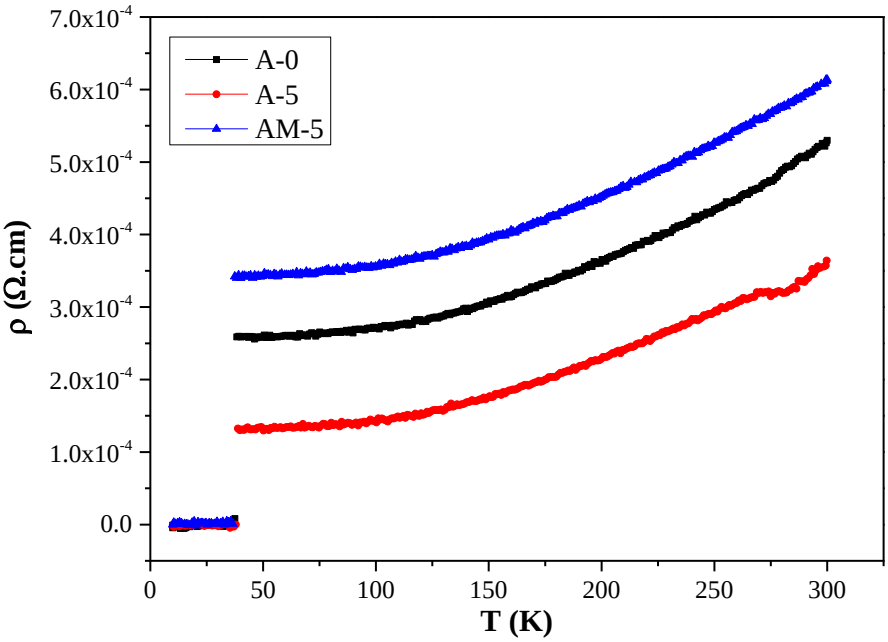


**Figure 8.** Resistivity versus temperature, $\rho(T)$ curves between 300 K and 10 K at B = 0 T for the A-0, A-5 and AM-5 samples.
***Şekil 8.*** *A-0, A-5 ve AM-5 örnekleri için 300 K ve 10 K arasında ve B = 0 T'de sıcaklığa karşı özdirenç, ρ(T) eğrileri.*

**Table 3.** The values of $\rho_{40K}$, $\rho_{300K}$, $\Delta\rho$, $\rho_0$ and *RRR* for the A-0, A-5 and AM-5 samples.
***Tablo 3.*** *A-0, A-5 ve AM-5 örnekleri için $\rho_{40K}$, $\rho_{300K}$, $\Delta\rho$, $\rho_0$ ve RRR değerleri.*

| Samples | $\rho_{40K}$ (μΩcm) | $\rho_{300K}$ (μΩcm) | $\Delta\rho$ (μΩcm) | $\rho_0$ (μΩcm) | *RRR* |
|---|---|---|---|---|---|
| A-0 | 258 | 529 | 271 | 4.09 | 2.05 |
| A-5 | 130 | 364 | 234 | 2.39 | 2.80 |
| AM-5 | 340 | 613 | 273 | 5.36 | 1.80 |

## 4. Conclusions
*4. Sonuçlar*

The influence of ball milling on some superconducting characteristics of the oleic acid added $MgB_2$ bulk samples prepared by two different ways was investigated in this research. The results show that ball milling process enhances the homogeneity and grain connectivity of the oleic acid added samples. In addition, the C substitution into the $MgB_2$ and the impurity scattering increase and thus the mean free path decreases. Ball milling also causes an increase in the amount of defects and disorders in $MgB_2$, operating as pinning centres. Thus, the $F_p$ and $J_c$ values of the ball milled samples at high magnetic fields increase while the $T_c$ values slightly decrease. Because the first method supports the ball milling effect on the C substitution into B sites and the homogenous distribution of the oleic acid addition in the structure, the ball milling process used in this study with a 1:20 powder mass-ball mass ratio and for 2 h with a rotation speed of 200 rpm is more effective to enhance the $J_c$ value at high fields for the samples produced with the first method, compared to the second one.

**Acknowledgement**
*Teşekkür*

The author would like to thank Tayfur Kucukomeroglu for his kind technical assistance. The Scientific Research Project Coordinatorship of Bayburt University supported this study with project number 2019/02-69001-02. The samples were made at Karadeniz Technical University in Trabzon, Turkey.

**Declaration of ethical code**
*Etik beyan*

The author of this article declares that the materials and methods used in this study do not require ethical committee approval and/or legal-specific permission.

**Conflicts of interest**
*Çıkar çatışması beyanı*

The author declares that there is no conflict of interest.

**References**
*Kaynaklar*

Bean, C. P. (1962). Magnetization of hard superconductors. Physical review letters, 8(6), 250. https://doi.org/10.1103/PhysRevLett.8.250

Buzea, C., & Yamashita, T. (2001). Review of the superconducting properties of MgB2. Superconductor Science and Technology, 14(11), R115. https://doi.org/10.1088/0953-2048/14/11/201

Das, S., Bernhard, C., & Varma, G. D. (2015). Effect of combined addition of graphene oxide and citric acid on superconducting properties of MgB2. Physica C: Superconductivity and its Applications, 509, 49-55. https://doi.org/10.1016/j.physc.2014.12.005

Eltsev, Y., Lee, S., Nakao, K., Chikumoto, N., Tajima, S., Koshizuka, N., & Murakami, M. (2002). Anisotropic superconducting properties of MgB2 single crystals probed by in-plane electrical transport measurements. Physical Review B, 65(14), 140501. https://doi.org/10.1103/PhysRevB.65.140501

Erdem, O., Abdioglu, M., Guner, S. B., Celik, S., & Kucukomeroglu, T. (2017). Improvement in levitation force performance of bulk MgB2 superconductors through coronene powder adding. Journal of Alloys and Compounds, 727, 1213-1220. https://doi.org/10.1016/j.jallcom.2017.08.242

Erdem, O., Guner, S. B., Celik, S., & Kucukomeroglu, T. (2020). Superconducting and levitation force characterisation of pyrene added MgB2 bulk superconductors. Cryogenics, 112, 103205. https://doi.org/10.1016/j.cryogenics.2020.103205

Erdem, O., & Yanmaz, E. (2015). Effect of Er doping on the superconducting properties of porous MgB2. Bulletin of Materials Science, 38(1), 89-93. https://doi.org/10.1007/s12034-014-0810-y

Erdem, O., & Yanmaz, E. (2017). Enhanced pinning properties of laser-irradiated bulk MgB2 superconductors. Journal of Superconductivity and Novel Magnetism, 30(3), 769-776. https://doi.org/10.1007/s10948-016-3777-7

Gozzelino, L., Gerbaldo, R., Ghigo, G., Laviano, F., Torsello, D., Bonino, V., ... & Badica, P. (2019). Passive magnetic shielding by machinable MgB2 bulks: measurements and numerical simulations. Superconductor Science and Technology, 32(3), 034004. https://doi.org/10.1088/1361-6668/aaf99e

Jiang, J., Senkowicz, B. J., Larbalestier, D. C., & Hellstrom, E. E. (2006). Influence of boron powder purification on the connectivity of bulk MgB2. Superconductor Science and Technology, 19(8), L33. https://doi.org/10.1088/0953-2048/19/8/L02

Kazakov, S. M., Puzniak, R., Rogacki, K., Mironov, A. V., Zhigadlo, N. D., Jun, J., ... & Karpinski, J. (2005). Carbon substitution in MgB2 single crystals: Structural and superconducting properties. Physical Review B, 71(2), 024533. https://doi.org/10.1103/PhysRevB.71.024533

Kimishima, Y., Takami, S., Okuda, T., Uehara, M., Kuramoto, T., & Sugiyama, Y. (2007). Complete flux jump in bulk MgB2 sintered under high pressure. Physica C: Superconductivity and its applications, 463, 281-285. https://doi.org/10.1016/j.physc.2007.03.492

Klöppel, S., Marian, A., Haberstroh, C., & Bruzek, C. E. (2021). Thermo-hydraulic and economic aspects of long-length high-power MgB2 superconducting cables. Cryogenics, 113, 103211. https://doi.org/10.1016/j.cryogenics.2020.103211

Kulich, M., Kováč, P., Hain, M., Rosová, A., & Dobročka, E. (2016). High density and connectivity of a MgB2 filament made using the internal magnesium diffusion technique. Superconductor Science and Technology, 29(3), 035004. https://doi.org/10.1088/0953-2048/29/3/035004

Laliena, C., Martínez, E., Angurel, L. A., & Navarro, R. (2015). Effect of ball milling and fatty acid addition on the properties of MgB2 wires. IEEE Transactions on Applied Superconductivity, 25(3), 1-4. https://doi.org/10.1109/TASC.2014.2364158

Liu, H. R., Xie, Z. W., Jin, L. H., Yang, F., Zhang, S. N., Wang, Q. Y., ... & Zhou, L. (2020). Improved superconducting properties in graphene-doped MgB2 bulks prepared by high energy ball milling. Journal of Materials Science: Materials in Electronics, 31(11), 8837-8843. https://doi.org/10.1007/s10854-020-03418-3

Majoros, M., Sumption, M. D., Parizh, M., Wan, F., Rindfleisch, M. A., Doll, D., ... & Collings, E. W. (2022). Magnetic, Mechanical and Thermal Modeling of Superconducting, Whole-Body, Actively Shielded, 3 T MRI Magnets Wound Using MgB2 Strands for Liquid Cryogen Free Operation. IEEE Transactions on Applied Superconductivity, 32(4), 1-4. https://doi.org/10.1109/TASC.2022.3147137

Martínez, E., Navarro, R., & Andrés, J. M. (2013). Improvement of the critical current density on in situ PIT processed Fe/MgB2 wires by oleic acid addition. Superconductor Science and Technology, 26(12), 125017. https://doi.org/10.1088/0953-2048/26/12/125017

Matsushita, T., Kiuchi, M., Yamamoto, A., Shimoyama, J. I., & Kishio, K. (2008). Essential factors for the critical current density in superconducting MgB2: connectivity and flux pinning by grain boundaries. Superconductor Science and Technology, 21(1), 015008. https://doi.org/10.1088/0953-2048/21/01/015008

Naito, T., Ogino, A., Fujishiro, H., & Awaji, S. (2020). Effects of Carbon Doping on Trapped Magnetic Field of MgB2 Bulk Prepared by in-situ Hot Isostatic Pressing Method. IEEE Transactions on Applied Superconductivity, 30(4), 1-6. https://doi.org/10.1109/TASC.2020.2985355

Sun, X. G., Yang, X. S., Pan, X. F., Xi, D., Wang, Q. Y., Yan, G., ... & Zhao, Y. (2019). Ex situ MgB2 superconducting tape with very high critical current density by using low-temperature sintering precursor powders. Journal of Superconductivity and Novel Magnetism, 32(5), 1225-1230. https://doi.org/10.1007/s10948-018-4861-y

Surdu, A. E., Hamdeh, H. H., Al-Omari, I. A., Sellmyer, D. J., Socrovisciuc, A. V., Prepelita, A. A., ... & Sidorenko, A. S. (2011). Enhancement of the critical current density in FeO-coated MgB2 thin films at high magnetic fields. Beilstein Journal of Nanotechnology, 2(1), 809-813. https://doi.org/10.3762/bjnano.2.89

Takenobu, T., Ito, T., Chi, D. H., Prassides, K., & Iwasa, Y. (2001). Intralayer carbon substitution in the MgB2 superconductor. Physical Review B, 64(13), 134513. https://doi.org/10.1103/PhysRevB.64.134513

Van Devener, B., Perez, J. P. L., & Anderson, S. L. (2009). Air-stable, unoxidized, hydrocarbon-dispersible boron nanoparticles. Journal of Materials Research, 24(11), 3462-3464. https://doi.org/10.1557/jmr.2009.0412

Wen, C., Liu, J., Yu, Z., Liu, J., Zhao, Z., & Wang, J. (2019). Research on superconducting magnet in a superconducting synchronous generator. Journal of Superconductivity and Novel Magnetism, 32(11), 3385-3395. https://doi.org/10.1007/s10948-019-5113-5

Wu, Y. F., Lu, Y. F., Yan, G., Li, J. S., Feng, Y., Tang, H. P., ... & Zhang, P. X. (2006). Improved superconducting properties in bulk MgB2 prepared by high-energy milling of Mg and B powders. Superconductor Science and Technology, 19(11), 1215. https://doi.org/10.1088/0953-2048/19/11/021

Ye, S. J., Matsumoto, A., Zhang, Y. C., & Kumakura, H. (2014). Strong enhancement of high-field critical current properties and irreversibility field of MgB2 superconducting wires by coronene active carbon source addition via the new B powder carbon-coating method. Superconductor Science and Technology, 27(8), 085012. https://doi.org/10.1088/0953-2048/27/8/085012